Isolation of a Californium(II) Crown-Ether Complex

Todd N. Poe,[1] Harry Ramanantoanina,[2] Joseph M. Sperling,[1] Hannah B. Wineinger,[1] Brian M. Rotermund,[1] Jacob Brannon,[1] Zhuanling Bai,[1] Benjamin Scheibe,[1] Nicholas Beck,[1] Brian N. Long,[1] Samantha Justiniano,[1] Thomas E. Albrecht-Schönzart,[1]* Cristian Celis-Barros[1]*

[1]Department of Chemistry and Biochemistry, Florida State University, Tallahassee, Florida 32306 USA

[2]Karlsruhe Institute of Technology, Institute for Nuclear Waste Disposal (INE), P.O. Box 3640, D-76021 Karlsruhe, Germany

*talbrechtschoenzart@gmail.com

*cristian.andree@gmail.com

ABSTRACT

Californium (Z = 98) is the first member of the actinide series displaying metastability of the 2+ oxidation state. Understanding the origin of this chemical behavior requires characterizing Cf^{II} materials, but isolating a complex with this state has remained elusive. The source of its inaccessibility arises from the intrinsic challenges of manipulating this unstable element as well as a lack of suitable reductants that do not reduce Cf^{III} to Cf^{0}. Herein we show that a Cf^{II} crown-ether complex, Cf(18-crown-6)I_2, can be prepared using an Al/Hg amalgam as a reductant. While spectroscopic evidence shows that Cf^{III} can be quantitatively reduced to Cf^{II}, rapid radiolytic re-oxidation back to the Cf^{III} parent occurs and co-crystallized mixtures of Cf^{II} and Cf^{III} complexes are isolated if the crystallization is not conducted over the Al/Hg amalgam. Quantum chemical calculations show that the Cf–ligand interactions are highly ionic and that 5*f*/6*d* mixing is absent,

resulting in remarkably weak 5*f*→5*f* transitions and an absorption spectrum dominated by 5*f*→6*d* transitions.

INTRODUCTION

Recent advances in heavy element chemistry spurred by innovative molecular design, new spectroscopic techniques, and relativistic theory have evolved our understanding of the divergence between the chemistries of 5*f* elements and their 4*f* counterparts. Historically the primary distinction between these two series has been that early actinides display facile redox chemistry compared to lanthanides with the exception of those with special electronic configurations such as Eu^{II} ($4f^{7}$) and Yb^{II} ($4f^{14}$).[1] This key attribute is largely lost in all trans-plutonium elements (excluding nobelium) where the most stable oxidation state is 3+ akin to lanthanides.[2] This has led to the notion that their chemistries are lanthanide-like. The combination of this bias with their scarcity, short half-lives, and need for specialized research facilities has further stymied progress in understanding these elements. However, it has been known for several decades that actinides from californium to nobelium have accessible 2+ oxidation states.[3] In fact, electro- and thermochemical measurements have shown a progressive stabilization of the 2+ state ultimately revealing that No^{II} is more stable than No^{III} by 1.45 V.[4–6]

Of late significant efforts have been dedicated to isolating complexes containing *f*-elements in either new or rare oxidation states for the purpose of determining their electronic configurations, bonding trends, spectroscopic features, and reactivity. Using strong reductants such as KC_8 and low-temperature reaction conditions, the first examples of Th^{II}, U^{II}, Np^{II}, and Pu^{II} tris-cyclopentadienyl derivatives such as $[Pu(Cp')_3]^{1-}$ (Cp' = trimethylsilylcyclopentadienyl) have been prepared, characterized, and their reactivities explored.[7–10] These studies inspired the pursuit of other molecular scaffolds for stabilizing U^{II} such as the U^{II} bis(amidate arene) $[U(TDA)_2]^{1-}$ (TDA

= N-(2,6-di-isopropylphenyl)pivalamido) that acts as U^{I} synthon because of the non-innocence of the ligand, as well as the monoarene [U((^{Ad,Me}ArO)$_3$mes)] that exhibits stabilization of U^{II} via δ-backbonding.[11,12] These reductive methods can also yield compounds whose oxidation states are difficult to describe such as [K(18-crown-6)(THF)$_2$]$_2$[U(η^6-$C_{14}H_{10}$)(η^4-$C_{14}H_{10}$)(μ-OMe)]$_2$·4THF.[13] Likewise, Cf^{II} complexes have been prepared in the gas phase as exemplified by reductive elimination of CH_3SO_2 from $Cf^{III}(CH_3SO_2)_4^-$ to yield $Cf^{II}(CH_3SO_2)_3^-$.[14]

The issue with applying the above synthetic methods to the preparation of low-valent trans-plutonium complexes is that unlike early actinides the standard reduction potential for $An^{III} \rightarrow An^{II}$ can be quite similar to the potential for $An^{III} \rightarrow An^0$. In fact, even with uranium the reaction of UCl_4 with $LiC_{10}H_8$ results in the formation of U^0 nanoparticles.[15] Thus, it would be expected that the reactions of alkali metal-based reagents with Cf^{III} should result in the formation of Cf^0 unless the supporting ligands prevent over reduction because the potential for $Cf^{III} \rightarrow Cf^{II}$ is −1.525 V, whereas the $Cf^{III} \rightarrow Cf^0$ potential is −2.01 V.[16,17] Moreover, for americium the potential for $Am^{III} \rightarrow Am^{II}$ is −2.28 V versus $Am^{III} \rightarrow Am^0$ at −2.00 V, rendering the formation of Am^0 at lower energy than Am^{II}.[18] Reagents such as KC_8 are expected to yield ca. 2.93 V of reduction potential and thus are anticipated to be too strong for preparing most trans-plutonium An^{II} complexes.

Lastly, one cannot neglect that all trans-plutonium isotopes have high specific activities and that both their ionizing radiation and concomitant formation of radiolysis products will influence the longevity of certain oxidation states. For example, radiolysis products rapidly reduce Bk^{IV} to Bk^{III}, but instead oxidize $Cf^{II}I_2$ to $Cf^{III}OI$ via the stunning α-particle induced abstraction of oxide from silica reaction vessels.[19,20] The latter provides an excellent illustration of the energetic differences between nuclear and chemical reactions. Taken together, there are two hurdles to overcome to successfully isolate a Cf^{II} complex. First, a reductant must be identified

that is strong enough to reduce Cf^{III} to Cf^{II} but does not over reduce it to Cf^{0}. Second, synthetic methodologies must be developed that allow for rapid complexation, reduction, and crystallization before radiolytic re-oxidation occurs. Herein, we show that Al/Hg amalgams can be used to achieve the proper reduction potential, and that crown ether ligands are appropriate for rapid crystallization of Cf^{II} complexes.

RESULTS AND DISCUSSION

Synthesis. We have previously shown that when Sm^{II} is coordinatively saturated by large crown-ether ligands such as dibenzo-30-crown-10 that the resultant complex is stable in aqueous media for days.[21] This is somewhat surprising because Sm^{II} normally reduces water and forms $\{Sm^{III}_2O_2\}$ oxo- or hydroxo-dimers. From electrochemical measurements it has been affirmed that the stability of Sm^{II} crown-ether complexes is kinetic in origin. This chemistry has been used to guide our synthetic efforts for Cf^{II} because of the similarities between the Sm^{III} to Sm^{II} standard reduction potential (−1.66 V) with that of californium.[16] Given the difficulties in preparing soluble and anhydrous trans-plutonium starting materials, this former observation suggests that a route that is tolerant to a small amount of water might be initially more flexible than strictly moisture and air-free methods.

After optimizing the following reaction with both samarium and americium as well as with dicyclohexano-18-crown-6, the desired Cf^{II} crown-ether complex, Cf^{II}(18-crown-6)I_2, was prepared via the reaction of $CfI_3 \cdot nH_2O$ ($n \leq 6$) with 18-crown-6 in the presence of $[NBu_4][BPh_4]$ over a large excess of Al/Hg amalgam in anhydrous acetonitrile. Solubility issues with the $[Cf^{III}(18\text{-crown-6})(H_2O)(CH_3CN)I]I_2$ complex that initially forms were eliminated by adding $[NBu_4][BPh_4]$ to the reaction mixture to inhibit ion pairing as was done in other Sm^{II} reactions.[22]

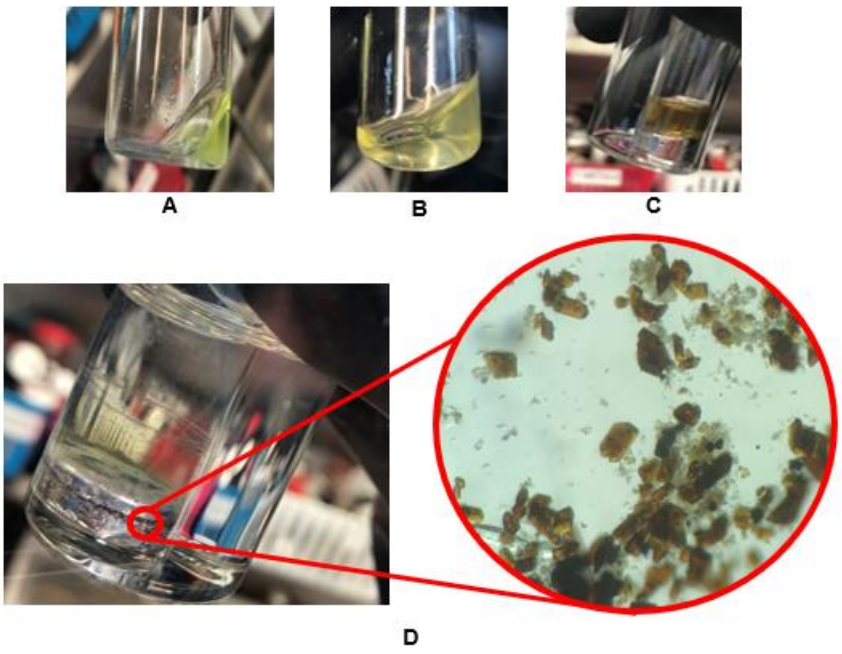

Figure 1: Reaction and isolation of Cf(18-crown-6)I_2. A) In a glovebox under argon atmosphere, dissolution of $CfI_3 \cdot nH_2O$ ($n \leq 6$) and two molar equivalents of $[NBu_4][BPh_4]$ in ~ 1 mL of acetonitrile yields a bright green solution. B) Addition of one molar equivalent of 18-crown-6 to the solution in (A) results in a shift to a bright yellow color. C) Finally, reduction of this solution over an excess of Al/Hg amalgam produces a peach-brown solution that is then placed over a separate Al/Hg amalgam in a reaction vial for vapor diffusion of 1:1 diethyl ether and pentane. D) Over the course of a few hours, red-brown crystals grow primarily between the amalgam and the wall of the glass vial, and the formation of $Al(OH)_3$ powder from the reduction of excess water is observed at the surface of the amalgam.

It is important to note that while the $CfI_3 \cdot nH_2O$ ($n \leq 6$) is obviously hydrated that this material has been dried in vacuo, and this process is known to convert hexahydrates to monohydrates.[23] $CfI_3 \cdot nH_2O$ ($n \leq 6$) rapidly decomposes in the presence of O_2 or even excess water (as does Cf(18-crown-6)I_2), thus these reactions are conducted in a glovebox under an argon atmosphere. No further removal of coordinated or lattice water is necessary because the Al/Hg amalgam also removes the water from the reaction mixture via its reduction and subsequent precipitation of $Al(OH)_3$ as shown in Figure 1C.

When $CfI_3 \cdot nH_2O$ ($n \leq 6$) is reacted with 18-crown-6 in the presence of $[NBu_4][BPh_4]$, a green-yellow solution forms that contains $[Cf^{III}(18\text{-crown-6})(H_2O)(CH_3CN)I]I_2$. Once this solution is placed over the Al/Hg amalgam and agitated, it begins to darken over the course of a

few minutes to a peach-brown color as shown in Figure 1C. We have evidence that [Cf^{III}(18-crown-6)(H_2O)(CH_3CN)I]I_2 is first reduced to [Cf^{II}(18-crown-6)(H_2O)$_2$(CH_3CN)]I_2, and that the water is lost to the amalgam to yield the desired Cf(18-crown-6)I_2 complex. It should be noted that if the mother liquor is removed from the amalgam at this stage its color will revert back to the original yellow-green color of the starting solution. While crystals can be isolated from this solution, they contain a mixture of Cf^{II} and Cf^{III} in the form of [Cf(18-crown-6)(H_2O)$_{2-x}$(CH_3CN)I_x]I_2.

This issue is circumvented by growing crystals over the amalgam itself via vapor diffusion of a 1:1 mixture of diethyl ether and pentane into the mother liquor at 0 ºC. Red-brown crystals of Cf(18-crown-6)I_2 primarily grow (in surprisingly high yield) between the amalgam and the wall of the glass vial as shown in Figure 1D. Even with this crystal growth method where a large excess of reductant is always present, these samples degrade at room temperature, 0 ºC, and even at −173 ºC in less than 16 hours because of radiolytic effects.

It should be noted that KC_8 can be used in the place of the Al/Hg amalgam, but as we discussed above, over reduction can occur rendering these reactions unpredictable. When this takes place, the californium becomes intercalated into the graphite and is difficult to extract. Given the scarcity of ^{249}Cf, the herculean efforts required to recycle it, and the real external radiation hazards that it poses to researchers even on small scales (ca. 5 mg), it is ill advised to utilize these overly strong reductants to prepare Cf^{II}.

Structure. Single crystal X-ray diffraction studies reveal that Cf(18-crown-6)I_2 (Figure 2B) adopts a structure-type first established with Ln^{II} cations (Ln^{II} = Eu, Sm, Yb, Dy, Tm) that has been the subject of recent investigations for single molecule magnetism with Tm(18-crown-6)I_2.[22,24,25] The Cf(18-crown-6)I_2 molecule consists of a Cf^{II} cation bound within the cavity of the

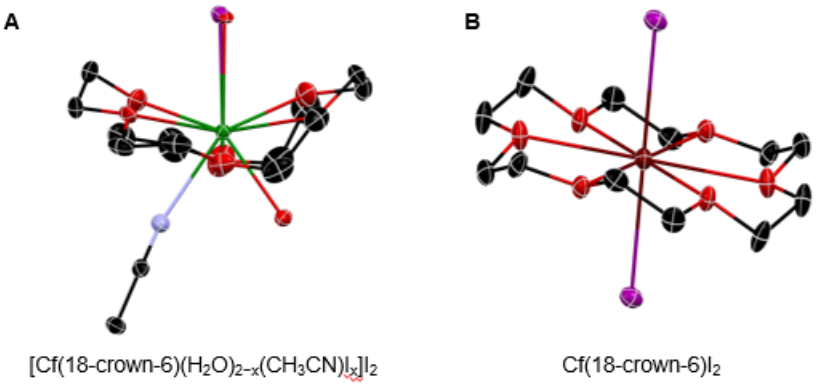

C

Bond Length Comparisons for M^{II}(18-crown-6)I_2

M^{II}	Sm (Å)	Eu (Å)	Dy (Å)	Tm (Å)	Yb (Å)	Cf (Å)
M1-O1	2.702(2)	2.6970(12)	2.645(8)	2.637(3)	2.6596(16)	2.685(5)
M1-O2	2.695(2)	2.6924(12)	2.616(8)	2.659(3)	2.6406(15)	2.684(5)
M1-O3	2.702(2)	2.7032(12)	2.614(8)	2.653(3)	2.6507(16)	2.666(5)
M1-I1	3.2363(3)	3.2153(3)	3.1383(10)	3.1171(3)	3.09211(18)	3.1563(4)
M1-I2	—	—		3.1172(3)	—	—

Figure 2. Crystal structures of [Cf(18-crown-6)$(H_2O)_{2-x}(CH_3CN)I_x]I_2$ and Cf(18-crown-6)I_2 with bond length table. A) Vapor diffusion of 1:1 diethyl ether and pentane over the peach-brown solution containing $[Cf(18\text{-crown-6})]^{2+}$ without the Al/Hg amalgam in the reaction vial yields crystals of the formula $[Cf(18\text{-crown-6})(H_2O)_{2-x}(CH_3CN)I_x]I_2$. The nine-coordinate metal complex in this crystal structure contains a partial occupancy in the apical position of ~69% O and 31% I. Green = Cf, purple = I, red = O, black = C, light blue = N. Hydrogen atoms have been omitted for clarity. Thermal ellipsoids are calculated at 50% probability. B) Vapor diffusion of 1:1 diethyl ether and pentane into the peach-brown solution over the Al/Hg amalgam yields crystals containing the 8-coordinate Cf(18-crown-6)I_2 metal complex. Brown = Cf, purple = I, red = O, black = Carbon. Hydrogen atoms have been omitted for clarity. Thermal ellipsoids are calculated at 50% probability. C) Comparison of bond lengths observed for Cf(18-crown-6)I_2 and comparable divalent lanthanide molecules of the formula Ln(18-crown-6)I_2, where Ln = Sm, Eu, Dy, Tm, Yb, reveals that both the Cf^{II}-O and Cf^{II}-I bond lengths fall between the bond lengths exhibited by the Eu^{II} and Dy^{II} analogues.

crown ether by the six etheric oxygen atoms and by two *trans* iodide anions. This yields a slightly distorted hexagonal bipyramidal environment where the Cf^{II} cation is located on an inversion center. Cf–O bond distances range from 2.685(5) to 2.666(5) Å and are slightly shorter than those found with Eu(II), but longer than those of Dy(II) as shown in Figure 2C. Although the Cf–O and Cf–I bonds are mostly ionic, there is a small covalent contribution to these bonds where the 5*f*-orbital participation is essentially negligible. The Cf–I bond distance is 3.1563(4) Å which is

notably shorter than that of Eu^{II}–I, but statistically longer than that observed for Dy^{II}–I.[22] The shortening of this bond is ascribed to the mixing of iodide $4p_z$ orbitals with Cf^{II} $6d_{z^2}$ orbitals (Figure 3A). Seeing as this is the first condensed-matter Cf^{II} molecule that has been isolated and characterized, these bond metrics help bracket the upper and lower limits of the ionic radius of Cf^{II}, which is currently not established.

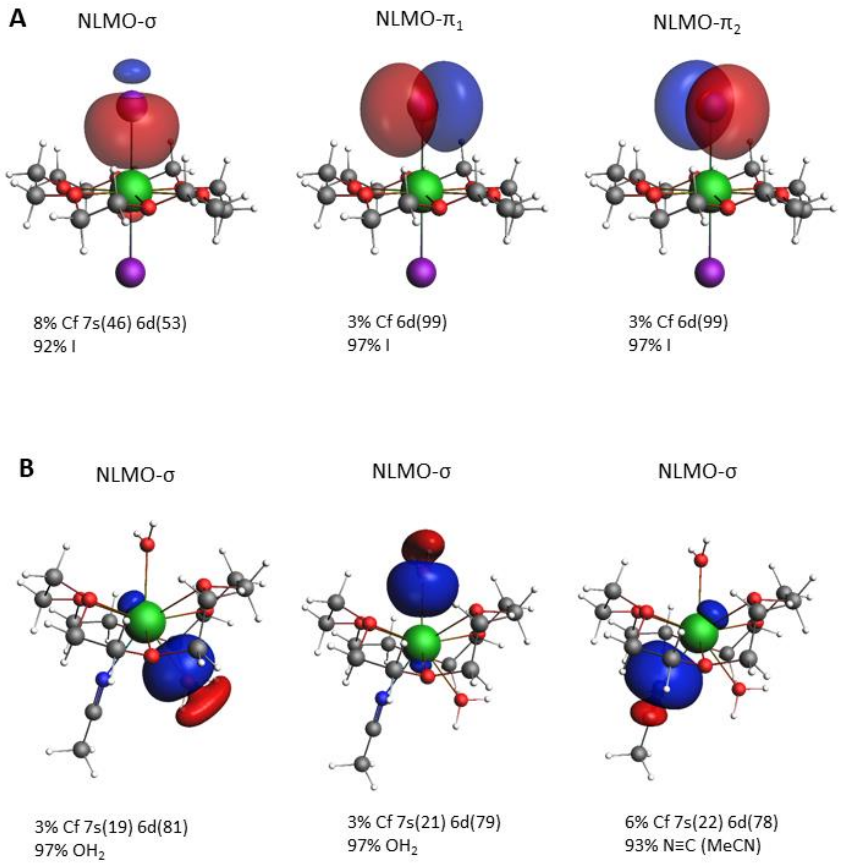

Figure 3: Natural localized molecular orbitals. Selected NLMOs showing the main interactions responsible for the Cf(III) – ligand bonding in A) $Cf(18\text{-crown-}6)I_2$ and B) $[Cf^{II}(18\text{-crown-}6)(H_2O)_2(CH_3CN)]^{2-}$.

As previously mentioned, crystals can be obtained in low yield from reaction mixtures where the mother liquor has been removed from the amalgam. These crystals, while complex in nature, shed some light on the reductive process. X-ray diffraction studies show that these crystals are composed of $[Cf(18\text{-crown-}6)(H_2O)_{2-x}(CH_3CN)I_x]I_2$ as shown in Figure 2. The structure

contains a mixture of an intermediate Cf^{II} complex, $[Cf(18\text{-crown-6})(H_2O)_2(CH_3CN)]I_2$, and the Cf^{III} parent $[Cf(18\text{-crown-6})(H_2O)(CH_3CN)I]I_2$. The key difference between these two complexes exists primarily in the apical position that can be occupied by either a H_2O molecule or an iodide anion. The structure refinement shows that the occupancy of the superimposed atomic positions are 0.6865(15) for the oxygen atom and 0.3135(15) for the iodide anion. In short, it contains ~69% Cf^{II} and 31% Cf^{III}.

Given that the solution spectrum did not show the presence of Cf^{III} and that O_2 has been excluded, two possible oxidants remain: water and radiolysis. In this study, the amount of water is low with no more than six equivalents of water present in the initial reaction, and any remaining water after the $CfI_3{\cdot}nH_2O$ is placed under vacuum is removed via reduction by the amalgam. Thus, we conclude from six replications of this experiment and numerous others, that radiolytic oxidation occurs and is the primary cause of oxidation. This latter result is expected given the high specific activity of ^{249}Cf.[3]

The presence of an oxygen atom in the apical position of $[Cf(18\text{-crown-6})(H_2O)_2(CH_3CN)]I_2$ does not necessarily mean that it is a water molecule. It could be a hydroxide anion instead, which would yield a Cf^{III} complex. However, computational analyses (Extended Data Table 1) show that a Cf^{III}–OH bond distance would be 2.098 Å resulting in a weighted bond distance of 2.407 Å for Cf^{III}–L (L = 69% OH^-, 31% I^-), which is much shorter than the observed distances of 2.705(11) and 2.742(2) Å for water and iodide, respectively. The same calculated weighted bond distance for Cf^{II}–L (L = 69% H_2O, 31% I^-) is 2.791 Å, which is in much better agreement with experimental data. This type of substitutional disorder is well precedented in general (*e.g.* the origin of the bond shift isomerization misidentification), but is also known from numerous actinide halide compounds such as $Pu_2[B_{12}O_{18}(OH)_4Br_2(H_2O)_3]{\cdot}0.5H_2O$ and

$Cm_2[B_{14}O_{20}(OH)_7(H_2O)_2Cl]$ where Br^-/H_2O or Cl^-/H_2O disorder occurs.[26,27] The present system is somewhat different from the latter of these examples and better parallels that of the Mo=O/Mo–Cl averaging where two different molecules are present in the same crystal structure on the same crystallographic sites.[28]

The structure of $[Cf(18\text{-crown-6})(H_2O)_2(CH_3CN)]I_2$ consists of a nine-coordinate Cf^{II} ion within a hula-hoop geometry. Similar to the $Cf(18\text{-crown-6})I_2$ structure, the "hoop" is formed from six approximately co-planar etheric oxygen atoms from the 18-crown-6 ligand. The apex is occupied by the aforementioned water molecule, and the two positions below the plane are filled by an acetonitrile molecule and a second water molecule as shown in Figure 2 with two outer-sphere iodide anions rounding out the asymmetric unit. This structure type is well established from lanthanide crown ether complexes and from this present study with Am^{III}.[29]

Spectroscopy. Room temperature solid-state absorption studies of single-crystals of $Cf(18\text{-crown-6})I_2$ yield broadband transitions in the UV-visible region as shown in Figure 4A. By comparison, typical solid-state absorption spectra of Cf^{3+}-containing compounds are dominated by distinct $5f \rightarrow 5f$ transitions.[30,31] Based on reported absorption data for Cf^{2+} binary halides, it is anticipated that compounds containing Cf^{2+} would also exhibit characteristic $5f \rightarrow 5f$ transitions.[20, 32-34] However, the broadband features observed in the experimental absorption spectra reported here are, in fact, $5f \rightarrow 6d$ transitions (Figure 4), and there is a notable lack of expected $5f \rightarrow 5f$ transitions. For comparison with the experimental data presented here as well as relevant literature data, Ligand-field DFT calculations were used to predict the absorption spectrum for this system (Figure 5). It is worth mentioning that the $5f \rightarrow 6d$ transitions reported in the literature for $CfCl_2$ and $CfBr_2$ in particular are higher in energy than the $5f \rightarrow 6d$ transitions exhibited by $Cf(18\text{-crown-6})I_2$. The expected $5f \rightarrow 5f$ transitions in this region are not observed as a result of either (or both)

the presence of a formal inversion center in the molecule or masking of the Laporte forbidden transitions by the electric dipole allowed 5*f*→6*d* transitions.

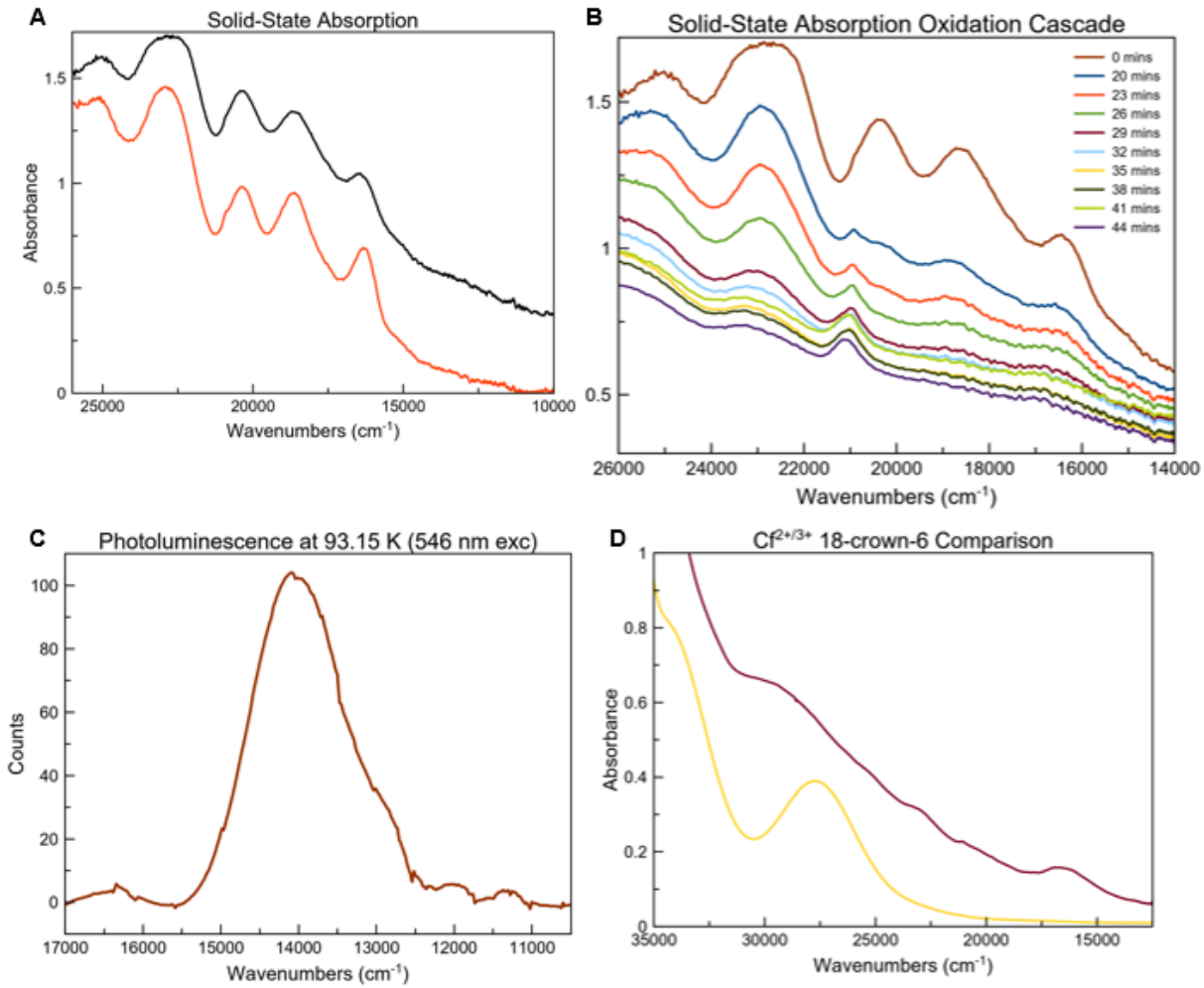

Figure 4: Solid-state and solution-phase UV-visible-NIR spectroscopy. A) Solid-state absorption of single-crystals of Cf(18-crown-6)I_2 exhibit broad, intense features in the UV and visible regions indicative of 5*f*→6*d* transitions. Black trace = ambient temperature, red trace = 93.15 K. B) At ambient conditions, the observed 5*f*→6*d* decrease as the Cf(18-crown-6)I_2 crystals oxidize and decompose over the course of 44 minutes along with the in-growth of a Cf^{3+} 5*f*→5*f* transition at 20,829 cm^{-1}. C) At room temperature, crystals of Cf(18-crown-6)I_2 do not photoluminescence, but at 93.15 K excitation with 546 nm light results in low intensity emission at 710 nm (14,087 cm^{-1}) similar to the emission observed from the reported Sm(18-crown-6)I_2 analogue. D) Solution-phase absorption measurements at ambient temperature reveal that the behavior of $[Cf(18\text{-crown-6})]^{2+}$ changes dramatically based on concentration of the ion, but that there is a clear difference in the features exhibited by the oxidized $[Cf(18\text{-crown-6})]^{3+}$ ion.

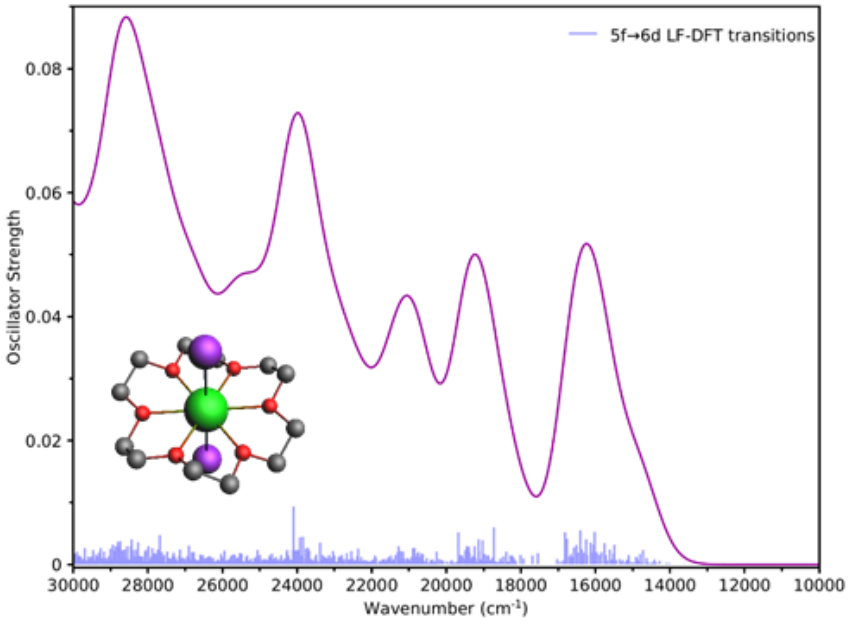

Figure 5: LFDFT absorption spectroscopy of [Cf^{II}(18-crown-6)I_2. Calculated absorption spectrum using the ligand-field DFT approach. Given that f-f transitions were extremely weak, they were excluded from the figure. The energy of the f-d transitions were overestimated significantly and were shifted to match the experimental spectrum. The presence of coordinating iodide ions generally causes issues predicting the intensity of the position of the d-orbitals.

The absorption spectrum collected at room temperature and 93.15 K display three main peaks indicative of 5*f*→6*d* transitions appearing in the visible region at 16,303 cm^{-1}, 18,662 cm^{-1}, and 20,368 cm^{-1}. These bands are produced by the excitation from different 5*f* orbitals to the lowest lying 6*d* orbitals, which in this case correspond to the $6d_{yz}$ and $6d_{xz}$ (Extended Data Figure 1). In addition, a shoulder resolves on the peak centered at 20,368 cm^{-1}. This shoulder is indicative of the oxidation of Cf^{2+}. Under the N_2 atmosphere of the temperature-controlled stage used for solid-state measurements, this oxidation is slowed such that reliable measurements can be obtained before complete oxidation of Cf^{2+} occurs. At room temperature, the oxidation occurs more rapidly under ambient conditions indicated by the increased intensity of the observed shoulder at 20,829

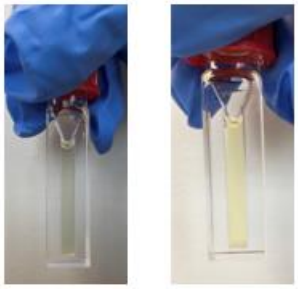

Figure 6: Acetonitrile solutions containing Cf^{2+} or Cf^{3+} and 18-crown-6. Reduction of $[Cf(18\text{-crown-6})]^{3+}$ in acetonitrile over the Al/Hg amalgam results in a color change from bright yellow to a dark peach-brown color. Dilution of this solution for spectroscopy results in a blue-green solution (left). Exposing this solution to oxygen yields a similar bright yellow solution (right) to that observed prior to reduction.

cm^{-1} and the gradual decrease of the $5f \rightarrow 6d$ transitions in the visible region as shown in Figure 4B.

The observed Cf^{2+} $5f \rightarrow 6d$ transitions are further supported by photoluminescence measurements of single crystals at 93.15 K. As shown in Figure 4C, excitation of these crystals with 546 nm (18,315 cm^{-1}) light yields broadband emission at 14,087 cm^{-1} (710 nm) which corresponds to emission of the first group of $5f \rightarrow 6d$ transitions (16,303 cm^{-1}). Compared to the photoluminescence observed from the isomorphous Sm(18-crown-6)I_2 under the same conditions, the emission exhibited by Cf(18-crown-6)I_2 is far less intense.[22]

The solution-phase absorption spectrum for this system corroborates the presence of Cf^{2+} prior to crystallization. As shown in Figure 4D, the absorption spectrum of $[Cf(18\text{-crown-6})_x]^{2+}$ in acetonitrile exhibits several broad features between 32,500 and 15,000 cm^{-1}. Most of these features can be attributed to the transitions identified in the solid-state absorption spectra of Cf(18-crown-6)I_2. However, there are notable differences in the spectra obtained from these two phases that are likely the result of competing coordination environments of the $[Cf(18\text{-crown-6})_x]^{2+}$ ion. An example of this is an observed color change that is dependent on the concentration of $[Cf(18\text{-crown-6})_x]^{2+}$ in solution. The more concentrated solution from which Cf(18-crown-6)I_2 crystallizes is a dark peach-brown color, but the color of this solution shifts dramatically when diluted with

acetonitrile resulting in a blue-green solution (Figure 6). In the presence of excess acetonitrile, it is probable that the more labile iodide ions would be displaced by solvent molecules. Given the possibility of different coordination environments in solution, the allowance of $5f \rightarrow 5f$ transitions cannot be overlooked. However, the pseudo-axial symmetry imposed by the coordination of the 18-crown-6 molecule restricts the overall intensity of these transitions compared to the dipole-allowed $5f \rightarrow 6d$ transitions (Extended Data Figure 2).

When the solution containing $[Cf(18\text{-crown-}6)_x]^{2+}$ is exposed to oxygen, a vivid color change from blue-green to bright yellow is observed resulting in the spectrum shown in Figure 6. Similar to studies with Sm^{2+}, the introduction of oxygen to this system rapidly oxidizes the divalent species to $[Cf(18\text{-crown-}6)_x]^{3+}$. The solution absorption spectrum obtained following this color change shows that the low energy features exhibited by the reduced species in acetonitrile are notably absent, and a broad, intense feature is observed at 27,758 cm^{-1} (360 nm) instead. This latter feature is comparable to the high energy transition displayed by $[Cf(18\text{-crown-}6)(H_2O)_{2-x}(CH_3CN)I_x]I_2$ in the same region (Extended Data Figure 3). Overall, the ambiguity of the solution-phase absorption data obtained for the divalent and trivalent species highlights the necessity for reliable solid-state structural evidence of the presence of Cf^{2+} in systems like the one reported here.

CONCLUSION

The isolation of $Cf(18\text{-crown-}6)I_2$ establishes an important precedent for stabilization of the 2+ oxidation state in the later actinides ($Z \geq 98$) in condensed-matter, molecular systems. Although radiolytic re-oxidation of Cf^{2+} is a significant hurdle to overcome, we have shown that the use of a more suitable reductant in the form of an Al/Hg amalgam is sufficient to reduce and maintain stability of the divalent state as well as prevent potential oxidants like water from

jeopardizing the integrity of Cf^{2+} in solution. Moreover, these conditions are appropriate and conducive to the isolation of crystalline products allowing for the solid-state characterization of Cf^{2+} molecules. Thus, the methods and results presented here are pivotal in the further exploration of the chemical behavior of californium and beyond.

REFERENCES

1. Clark, D. L. Chemical Complexities of Plutonium. *Los Alamos Sci.* 364–381 (2000).

2. Morss, L. R., Edelstein, N. M. & Fuger, J. *The Chemistry of the Actinide and Transactinide Elements*. (Springer, 2010).

3. Haire, R. G. Californium. in *The Chemistry of the Actinide and Transactinide Elements* (eds. Morss, L. R., Edelstein, N. M. & Fuger, J.) 1499–1576 (Springer, 2010).

4. Maly, J., Sikkeland, T., Silva, R. & Ghiorso, A. Nobelium: Tracer chemistry of the divalent and trivalent ions. *Science (80-.).* **160**, 1114–1115 (1968).

5. Silva, R. J. Fermium, Mendelevium, Nobelium, and Lawrencium. in *The Chemistry of the Actinide and Transactinide Elements* (eds. Morss, L. R., Edelstein, N. M. & Fuger, J.) 1621–1652 (Springer, 2010).

6. Mikheev, N. B., Auerman, L. N., Rumer, I. A., Kamenskaya, A. N. & Kazakevich, M. Z. The anomalous stabilisation of the oxidation state 2+ of lanthanides and actinides. *Russ. Chem. Rev.* **61**, 990–998 (1992).

7. Langeslay, R. R., Fieser, M. E., Ziller, J. W., Furche, F. & Evans, W. J. Synthesis, structure, and reactivity of crystalline molecular complexes of the $\{[C_5H_3(SiMe_3)_2]_3Th\}^{1-}$ anion containing thorium in the formal +2 oxidation state. *Chem. Sci.* **6**, 517–521 (2014).

8. Woen, D. H. & Evans, W. J. Expanding the + 2 Oxidation State of the Rare-Earth Metals, Uranium, and Thorium in Molecular Complexes. *Handb. Phys. Chem. Rare Earths* **50**, 337–394 (2016).

9. Su, J. *et al.* Identification of the Formal +2 Oxidation State of Neptunium: Synthesis and Structural Characterization of $\{Np^{II}[C_5H_3(SiMe_3)_2]_3\}^{1-}$. *J. Am. Chem. Soc.* **140**, 7425–7428 (2018).

10. Windorff, C. J. *et al.* Identification of the Formal +2 Oxidation State of Plutonium: Synthesis and Characterization of $\{Pu^{II}[C_5H_3(SiMe_3)_2]_3\}^{-}$. *J. Am. Chem. Soc.* **139**, 3970–3973 (2017).

11. Straub, M. D. *et al.* A Uranium(II) Arene Complex That Acts as a Uranium(I) Synthon. *J. Am. Chem. Soc.* **143**, 19748–19760 (2021).

12. Lapierre, H. S., Kameo, H., Halter, D. P., Heinemann, F. W. & Meyer, K. Coordination and Redox Isomerization in the Reduction of a Uranium(III) Monoarene Complex. *Angew. Chemie Int. Ed.* **53**, 7154–7157 (2014).

13. Murillo, J. *et al.* Actinide arene-metalates: ion pairing effects on the electronic structure of unsupported uranium–arenide sandwich complexes. *Chem. Sci.* **12**, 13360–13372 (2021).

14. Dau, P. D., Shuh, D. K., Sturzbecher-Hoehne, M., Abergel, R. J. & Gibson, J. K. Divalent and trivalent gas-phase coordination complexes of californium: Evaluating the stability of Cf(II). *Dalt. Trans.* **45**, 12338–12345 (2016).

15. Schöttle, C. *et al.* Nanosized Gadolinium and Uranium - Two Representatives of High-Reactivity Lanthanide and Actinide Metal Nanoparticles. *ACS Omega* **2**, 9144–9149

(2017).

16. Marsh, M. L. *et al.* Electrochemical Studies of Selected Lanthanide and Californium Cryptates. *Inorg. Chem.* **58**, 9602–9612 (2019).

17. David, F., Samhoun, K., Guillaumont, R. & Edelstein, N. Thermodynamic properties of 5f elements. *J. Inorg. Nucl. Chem.* **40**, 69–74 (1978).

18. Bard, A. J. *Standard Potentials in Aqueous Solution*. (International Union of Pure and Applied Chemistry, 1985).

19. Silver, M. A. *et al.* Electronic Structure and Properties of Berkelium Iodates. *J. Am. Chem. Soc.* **139**, 13361–13375 (2017).

20. Wild, J. F. *et al.* Studies of californium(II) and (III) iodides. *J. Inorg. Nucl. Chem.* **40**, 811–817 (1978).

21. White, F. D. *et al.* Molecular and Electronic Structure, and Hydrolytic Reactivity of a Samarium(II) Crown Ether Complex. *Inorg. Chem.* **58**, 3457–3465 (2019).

22. Poe, T. N., Molinari, S., Justiniano, S., McLeod, G. M. & Albrecht-Schönzart, T. E. Structural and Spectroscopic Analysis of Ln(II) 18-crown-6 and benzo-18-crown-6 Complexes (Ln = Sm, Eu, Yb). *Cryst. Growth Des.* **22**, 842–852 (2022).

23. Brown, B. D. *et al.* The preparation and crystallographic properties of certain lanthanide and actinide tribromides and tribromide hexahydrates. *J. Chem. Soc. A Inorganic, Phys. Theor.* **67**, 1889–1894 (1968).

24. Xémard, M. *et al.* Divalent Thulium Crown Ether Complexes with Field-Induced Slow Magnetic Relaxation. *Inorg. Chem.* **58**, 2872–2880 (2019).

25. Merzlyakova, E. *et al.* 18-Crown-6 Coordinated Metal Halides with Bright Luminescence and Nonlinear Optical Effects. *J. Am. Chem. Soc.* **143**, 798–804 (2021).

26. Wang, S., Alekseev, E. V., Depmeier, W. & Albrecht-Schmitt, T. E. Surprising coordination for plutonium in the first plutonium(III) borate. *Inorg. Chem.* **50**, 2079–2081 (2011).

27. Polinski, M. J. *et al.* Differentiating between trivalent lanthanides and actinides. *J. Am. Chem. Soc.* **134**, 10682–10692 (2012).

28. Mironov, Y. V., Cody, J. A., Albrecht-Schmitt, T. E. & Ibers, J. A. Cocrystallized mixtures and multiple geometries: Syntheses, structures, and NMR spectroscopy of the Re_6 clusters $[NMe_4]_4[Re_6(Te_{(8-n)}Se_{(n)})(CN)_6]$ (n = 0-8). *J. Am. Chem. Soc.* **119**, 493–498 (1997).

29. Rogers, R. D., Rollins, A. N., Etzenhouser, R. D., Voss, E. J. & Bauer, C. B. Structural Investigation into the Steric Control of Polyether Complexation in the Lanthanide Series: Macrocyclic 18-Crown-6 versus Acyclic Pentaethylene Glycol. *Inorg. Chem.* **32**, 3451–3462 (1993).

30. Cary, S. K. *et al.* A series of dithiocarbamates for americium, curium, and californium. *Dalt. Trans.* **47**, 14452–14461 (2018).

31. Sperling, J. *et al.* Pressure-Induced Spectroscopic Changes in a Californium 1D Material Are Twice as Large as Found in the Holmium Analog. *Inorg. Chem.* **59**, 10794–10801 (2020).

32. Peterson, J. R., Fellows, R. L., Young, J. P. & Haire, R. G. Stabilization of californium(II)

in the solid-state – californium dichloride, $^{249}CfCl_2$. *Radiochem. Radioanal. Lett.* **31**, 277–282 (1977).

33. Peterson, J. R. & Baybarz, R. D. The stabilization of divalent californium in the solid state: Californium dibromide. *Inorg. Nucl. Chem. Lett.* **8**, 423–431 (1972).

34. Young, J. P., Vander Sluis, K. L., Werner, G. K., Peterson, J. R. & Noé, M. High temperature spectroscopic and X-ray diffraction studies of californium tribromide: Proof of thermal reduction to californium(II). *J. Inorg. Nucl. Chem.* **37**, 2497–2501 (1975).

Author Information:

Corresponding Author

*Email: cristian.andree@gmail.com

*Email: talbrechtschoenzart@gmail.com

ORCID

Todd N. Poe: 0000-0001-7014-8850

Harry Ramanantoanina: 0000-0002-2086-6958

Joseph M. Sperling: 0000-0003-1916-5633

Hannah B. Wineinger: 0000-0003-4070-999X

Brian M. Rotermund: 0000-0002-2379-0119

Jacob Brannon: 0000-0001-7786-127X

Zhuanling Bai: 0000-0003-1412-2087

Benjamin Scheibe: 0000-0002-4665-6289

Nicholas Beck: 0000-0001-5687-192X

Brian N. Long: 0000-0003-4410-4509

Samantha Justiniano: 0000-0001-6117-4432

Thomas E. Albrecht-Schönzart: 0000-0002-2989-3311

Cristian Celis-Barros: 0000-0002-4685-5229

Notes

The authors declare no competing financial interest.

Acknowledgements.

This research was supported by the U.S. Department of Energy, Office of Science, Office of Basic Energy Sciences, Heavy Elements Chemistry Program, under Award DE-FG02- 13ER16414.

METHODS

Experimental

Caution! Americium-243 ($t_{1/2}$= 7364 years; specific activity = 200 mCi/g) is a strong α emitter (up to ~5.35 MeV) with γ radiation also associated with it (max peak ~75 keV), presenting internal and external radiotoxic hazards. The daughter isotope neptunium-239 ($t_{1/2}$ = 2.356 days; specific activity = 232 kCi/g) represents roughly half of the activity of the material once secular equilibrium is reached within about 2 weeks and emits powerful β particles, γ radiation, and X-rays. ^{249}Cf ($t_{1/2}$= 351 years; specific activity = 4.09 Ci/g) is a potentially significant internal and external radiologic hazard due to its 5.8 MeV α-particles (82.2% branch) and high energy γ-rays with 388 keV (66% branch) associated with it. The daughter of ^{249}Cf is ^{245}Cm ($t_{1/2}$ = 8,423 years; specific activity 173 mCi/g) and is an internal radiologic hazard from 5.36 MeV (93.2% branch) α-particles. Radioactive materials were handled with care at a Category II radiologic facility.

Materials. The $^{249}CfCl_3$ used in this experiment was isolated as a solid residue following purification procedures. The $^{243}AmCl_3$ used in this experiment was acquired from an Am stock solution in 2M HCl. DyI_2 (Sigma-Aldrich, 99%) was used as received. 18-crown-6 (Sigma-Aldrich, 99%) and tetrabutylammonium tetraphenylborate (Sigma-Aldrich, 99%) were used as received. Dicyclohexano-18-crown-6 (98%) was acquired as a mixture of cis-isomers from Sigma-Aldrich. The cis-syn-cis and cis-anti-cis isomers were separated from one another using the procedure established by Izatt and coworkers.[1] Hydroiodic acid (contains no stabilizer, distilled, 57 wt. % in H_2O, 99.99% trace metals basis, Sigma-Aldrich) was stored in a freezer at less than 0 °C until it was used. Ammonium hydroxide (28% NH_3 in H_2O, ≥ 99.99% trace metals basis, Sigma-Aldrich) was used as received. Diethyl ether (VWR, anhydrous ≥ 99.0% stabilized) was used as received for all manipulations on the benchtop. For manipulations in the glovebox, diethyl ether and acetonitrile (Sigma-Aldrich, anhydrous, 99.8%) were dried over sodium (Sigma-Aldrich, cubes, contains mineral oil, 99.9% trace metals basis) and benzophenone (Sigma-Aldrich, 99%) and CaH_2 (Sigma-Aldrich, reagent grade, 95% (gas-volumetric)), respectively, before being stored in a glovebox under an argon atmosphere over activated molecular sieves (3 Å, 4-8 mesh, Sigma-Aldrich). The Al/Hg amalgam was prepared as follows: Aluminum (Sigma-Aldrich, beads, 5-15 mm, 99.9% trace metals basis) was charged in a 100 mL Schlenk flask and submerged in concentrated HCl. Vigorous bubbling occurred as the oxide coating was stripped from the aluminum beads. The flask was stirred vigorously by hand for five minutes. The solution was then carefully decanted. The aluminum beads were washed 3 times with diethyl ether and then the entire flask was placed under vacuum overnight. The flask was then pumped into a glovebox under and argon atmosphere. In a 20 mL scintillation vial, enough Hg metal (Sigma-Aldrich, ≥ 99.99% trace metals basis) to just cover the bottom of the vial was added. Three aluminum beads were removed

from the Schlenk flask and careful placed over the mercury. The vial was capped and placed on a hot plate and heated to 250 °C. The amalgam was kept heated overnight and stirred occasionally. Eventually, aluminum began to dissolve in the mercury forming a dull gray, liquid Al/Hg amalgam.

Synthesis of [Cf(18-crown-6)(H_2O)$_{2-x}$(CH_3CN)I_x]I_2. In a fume hood, approximately 4.0 mg of $CfCl_3 \bullet nH_2O$ (0.016 mmol) was dissolved in 2 mL of 2 M HCl. This solution was transferred to a 15 mL centrifuge tube. An equivalent volume (2 mL) of concentrated ammonium hydroxide solution was added to the centrifuge tube and agitated resulting in a light green precipitate in the form of $Cf(OH)_3$. The mother liquor was separated by centrifugation, and the solid was washed with 4 mL of DI H_2O. These washings were completed in triplicate. After removing the final H_2O washing, the $Cf(OH)_3$ solid was dissolved in 4 drops of concentrated HI. This solution was transferred to a 20 mL scintillation vial. The solution was dried under a gentle stream of N_2 gas resulting in a black residue. The residue was washed three times with 2 mL fractions of diethyl ether and agitated vigorously with a plastic spatula to remove excess iodine. The washings were each carefully pipetted away, and after the third washing, the resulting yellow-green powder (putative $CfI_3 \bullet nH_2O$) was immediately placed under vacuum in a glovebox antechamber for 40 minutes. After 40 minutes, the $CfI_3 \bullet nH_2O$ was brought into the glovebox and immediately dissolved in 0.5 mL of acetonitrile resulting in a light green solution. Separately, 18.1 mg (0.032 mmol) of tetrabutylammonium tetraphenylborate was dissolved dropwise in acetonitrile and added to the solution containing CfI_3. Again, separately, 4.4 mg (0.017 mmol) of 18-crown-6 was dissolved in acetonitrile dropwise and added to the vial containing CfI_3. The solution was stirred gently and remained a light green color. This solution was then transferred to a 20 mL scintillation vial containing an Al/Hg amalgam. The vial was capped and agitated vigorously. Over the course

of five minutes, the solution slowly transitioned from a light green color to a light peach-brown color. This solution was separated from the amalgam *via* pipette, and the solution was centrifuged to remove excess $Al(OH)_3$ from the amalgam. This solution was transferred to a 6 mL shell vial that was inserted in a 20 mL scintillation vial. The outer scintillation vial was filled to 75% capacity with a 1:1 pentane-diethyl ether solution and capped for vapor diffusion. Overnight a yellowish solid precipitated. Amidst the yellow solid were small yellow-green rhombohedral crystals of $[Cf(18\text{-crown-6})(H_2O)_{2-x}(CH_3CN)I_x]I_2$ crystallizing in low yield (< 10%).

Synthesis of Cf(18-crown-6)I₂. Synthesis of putative $CfI_3 \bullet nH_2O$ was carried out as described for the reaction yielding $[Cf(18\text{-crown-6})(H_2O)_{2-x}(CH_3CN)I_x]I_2$. The $CfI_3 \bullet nH_2O$ was once again dried in vacuo in the antechamber of a glovebox before being introduced to the argon atmosphere of the glovebox. The yellow-green $CfI_3 \bullet nH_2O$ powder was dissolved in 1 mL of acetonitrile resulting in a light green solution. This solution was pipetted over 24.3 mg (0.043 mmol) of $[NBu_4][BPh_4]$ in a 6 mL glass scintillation vial and agitated to allow for dissolution of all solids. The same solution was then pipetted over 8.1 mg (0.031 mmol) 18-crown-6 and agitated to allow dissolution of the solid crown ether. No evident change in the color of the solution was observed. This solution was then pipetted over an Al/Hg amalgam in a 20 mL scintillation vial. The vial was capped and then agitated vigorously. Over the course of 10 minutes, the solution shifted to a dark peach-brown color, indicating reduction of the Cf^{3+} to Cf^{2+}. This solution was transferred to a 5 mL centrifuge tube and centrifuged to separate out solid $Al(OH)_3$ generated by the amalgam. Meanwhile a second amalgam prepared in advance from 1 mL of Hg (measured with a volumetric pipette) and an excess of Al metal was stored inside of a 6 mL glass shell vial that was inserted inside a 20 mL glass scintillation vial. After centrifugation, the solution was pipetted over the Al/Hg amalgam inside the 6 mL shell vial. The outer 20 mL vial was filled to 75% capacity

with a 1:1 solution of diethyl ether and pentane and capped for vapor diffusion. The solution was stored on a cold plate at 0 °C. Over the course of the next 4 hours, reddish-brown crystals of Cf(18-crown-6)I_2 formed, first around the Al/Hg amalgam where it contacted the glass of the shell vial, and then along the sides of the glass vial as well. Crystalline yield was approximately 50%.

Synthesis of [Am(cis-syn-cis-dicyclohexano-18-crown-6)(H_2O)(CH_3CN)I]I_2 • CH_3CN. Preparation of AmI_3 • nH_2O (n ≤ 6) was performed as described for CfI_3 • nH_2O (n ≤ 6). The AmI_3 • nH_2O (n ≤ 6) was transferred to a 20 mL glass scintillation vial which was then placed into the antechamber of an argon atmosphere glovebox and left under vacuum for 40 minutes. Once inside the glovebox, the AmI_3 • xH_2O powder was dissolved dropwise in acetonitrile with gentle stirring until completely dissolved. A pale-yellow solution formed. Separately, the *cis-syn-cis* isomer of dicyclohexano-18-crown-6 (7.8 mg, 0.021 mmol) was dissolved in in THF by dropwise addition of the solvent. Addition of the crown ether to the solution containing ^{243}Am resulted in a more intensely yellow colored solution. The solution was transferred to a 6 mL shell vial that was inserted into a 20 mL scintillation vial. The outer scintillation vial was filled to 75% capacity with diethyl ether and capped for vapor diffusion. Colorless, thin plate crystals of [Am(*cis-syn-cis*-dicyclohexano-18-crown-6)(H_2O)(CH_3CN)I]I_2 • CH_3CN formed overnight in low yield (< 10%). The crystal structure of [Am(*cis-syn-cis*-dicyclohexano-18-crown-6)(H_2O)(CH_3CN)I]I_2 • CH_3CN is shown in Extended Data Figure 4 along with a table of associated bond lengths. Solid-state absorption data collected from single-crystals of [Am(*cis-syn-cis*-dicyclohexano-18-crown-6)(H_2O)(CH_3CN)I]I_2 • CH_3CN appear in Extended Data Figure 5.

Preparation of Dy(18-crown-6)I_2. In a glovebox under an argon atmosphere, a 20 mL glass scintillation vial was charged with 20.0 mg of DyI_2. Then, 3 mL of cold (−30 °C) DME was added to the vial and swirled to encourage dissolution of the DyI_2. The dissolution process was slow, and

the solution began to turn a shade of dark green. The reaction vial was stored in a glovebox freezer at −30 °C to maintain stability of Dy^{2+} in solution. Every 10 minutes, the vial was removed from the freezer and a metal spatula was used to grind the remaining solid to encourage further dissolution of the DyI_2. The solution was then gently swirled and replaced in the freezer for another 10-minute period. This was repeated until all solids dissolved, resulting in a dark green solution. Separately, 12.7 mg of 18-crown-6 was dissolved in 3 mL of cold (−30 °C) toluene to create a stock solution and then stored in a glovebox freezer at −30 °C to maintain the temperature of the solution. Once both solutions were prepared and chilled to −30 °C, they were removed from the glovebox freezer. A disposable glass pipette was used to transfer 3 drops of the toluene solution containing 18-crown-6 to the DME solution containing DyI_2. Neither solution was stirred. Both solutions were then carefully (avoiding agitation of the solution) replaced in the glovebox freezer to maintain a solution temperature of −30 °C. Both solutions were allowed to sit in the freezer for 5 minutes untouched. Then, the solutions were carefully removed from the freezer to avoid agitation, and 3 drops of the toluene stock solution containing 18-crown-6 was again added to the solution containing DyI_2. This process was repeated continually avoiding agitation of the DyI_2 solution at all costs. Additions of the 18-crown-6 stock solution yielded a dark brownish-green precipitate almost immediately. After the slow, dropwise addition of almost half of the stock solution described previously, dark green microcrystals began to form on the walls of the glass scintillation vial. Slow, dropwise addition of the ligand solution sometimes resulted in crystals of Dy(18-crown-6)I_2 large enough for single-crystal x-ray diffraction studies, but total crystalline yield was low (< 20%). Further characterization and interpretation of Dy(18-crown-6)I_2 will reported elsewhere, but the crystal structure is crucial to the bond length comparisons for Cf(18-crown-6)I_2.

Crystallography. Crystals of all three compounds were isolated in a glovebox under an argon atmosphere and placed on a glass slide under immersion oil before being transferred to a microscope on the benchtop. Single crystals were then mounted on 75 μm inner diameter MiTeGen loops before being transferred to the goniometer of a Bruker D8 Quest Single Crystal X-ray Diffractometer with a IμS X-ray source (Mo Kα; λ = 0.71073 Å). A stream of N_2 gas was flowed over the crystals to preserve crystallinity and regulate the temperature of the sample. All collections were performed at 100.00 K. Subsequent data integration was performed using APEXIII software, and space group determination was performed using xprep. The following structure refinement was completed with the SHELXTL suite using the OLEX2 GUI.[2,3]

Spectroscopy. For solid-state spectroscopy, slides containing crystals of each compound under immersion oil were prepared in a glovebox under argon atmosphere before being transferred to the stage of a Craic Technologies 20/20 PVTM Dual Microspectrophotometer with a 75 W xenon lamp used for absorption spectroscopy. A Linkham temperature-controlled stage was utilized to study the behavior of both compounds at room and cold temperatures. Measurements were collected at ambient temperature and conditions before being transferred to the temperature-controlled stage under a blanket of N_2 gas. The stage was cooled at a rate of 5 °C per minute to −180 °C (93.15 K) and was allowed to equilibrate for five minutes before measurement. For solution-phase spectroscopy, samples were isolated in a glovebox under an argon atmosphere and sealed in quartz cuvettes (Starna cells, 0.4 cm path length) and then transferred to an Agilent Technologies Cary Series UV-Vis-NIR Spectrophotometer (Cary 6000i) for measurements. All solution-phase experiments were conducted at ambient temperature.

Computational Methods

Geometry Optimization. Given that the $[Cf(18\text{-crown-6})(H_2O)_{2-x}(CH_3CN)I_x]I_2$ crystal structure presents uncertainty on the nature of the capping ligand, three different structures were considered for geometry optimizations. Two of these correspond to an oxygen atom in the apical position in the form of a water molecule and a hydroxide anion, whereas the third structure includes the iodide anion as capping ligand. To reproduce properly the Cf–O bond lengths, 13 iodide ions surrounding the molecule in the crystal structure had to be incorporated (Extended Data Figure 6). Extended Data Table 1 shows a comparison between the experimental and theoretical bond lengths with and without the inclusion of the surrounding iodide ions. Our theoretical structures suggest that the oxygen in the apical position corresponds to a water molecule because a hydroxide anion should display a significantly shorter experimental bond length.

These calculations were performed in the ADF engine of AMS2021.[4] The generalized gradient approximation (GGA) PBE functional was used for this task along with the Slater-type orbital (STO)-DZ basis set for H, N, and C atoms, and STO-TZP for Cf, O, and I atoms. Scalar relativistic effects were included using the ZORA approximation as implemented in ADF.[5] For those calculations involving surrounding counter ions, the position of iodide anions were constrained to simulate the crystal packing.

Ligand Field DFT (LFDFT). The LFDFT approach has been used widely to reproduce the electronic structure of f-element complexes of mostly lanthanides but has also been applied to actinide complexes.[6-9] The inability of TD-DFT to predict multiplet electronic structure due to the lack of static correlation makes the LFDFT a more appropriate model, which account for both static and to a certain extent dynamic correlation.

The intensities associated with the excitation spectra were calculated using the oscillator strengths $f_{a,b}$ of an $a \rightarrow b$ electron transition, with a and b representing the initial final electronic

states (in atomic units): $f_{a,b} = \frac{2}{3}\Delta E_{a,b}\langle a|\boldsymbol{\mu}|b\rangle^2$, where the electric transition dipole moments were formulated in the dipole-length form ($\boldsymbol{\mu} = -r$). The non-zero oscillator strengths for 5*f*–5*f* transitions arise from the mixing between actinide 5*f* states and 6d or other ligand states in a non-centrosymmetric ligand-field regime. The ligand states for the actinide complexes are referred to the one-electron ligand-to-metal charge transfer states that possess large parentage of ligands 2*p* orbitals. We note that we use a static model somewhat equivalent to the Judd-Ofelt model,[10,11] where non-zero oscillator strengths existed through parity mixing that is due to the coordination geometry of the actinide ion. Thus, dynamical effects (eg. vibrations) were not considered in our calculations.

The calculated ligand field parameters for Cf(18-crown-6)I_2 in a $5f^{10}$ configuration at the PBE0/STO-TZP were: F^2 (*f*,*f*) = 9.7636 eV; F^4 (*f*,*f*) = 6.3244 eV; F^6 (*f*,*f*) = 4.6274 eV; ζ_{SO} (5*f*) = 0.4281 eV. For the $5f^9 6d^1$ configuration: F^2 (*f*,*f*) = 7.0900 eV; F^4 (*f*,*f*) = 4.6113 eV; F^6 (*f*,*f*) = 3.3802 eV; ζ_{SO} (5*f*) = 0.3778 eV; F^2 (*f*,*d*) = 0.4393 eV; F^4 (*f*,*d*) = 0.1743 eV; G^1 (*f*,*d*) = 0.1923 eV; G^3 (*f*,*d*) = 0.1319 eV; G^5 (*f*,*d*) = 0.0962 eV; ζ_{SO} (6*d*) = 0.0269 eV.

Molecular orbital localization. The Kohn-Sham orbitals obtained from single point calculations were used to obtain the Natural Localized Molecular Orbitals using the NBO module included in ADF.[12] The single point calculation was performed using the hybrid GGA PBE0 functional in conjunction with the STO-TZP basis set for all atoms except Cf and I, where the STO-TZ2P basis set was used.

Complete active space self-consistent field (CASSCF). Spin-orbit CASSCF calculations were performed in ORCA 5.0.2 at the PBE0/TZVP level of theory (except H atoms for which we used the small SVP basis set).[13] Scalar relativistic effects were included via the Douglas-Kroll-

Hess (DKH) Hamiltonian and spin-orbit coupling via state interaction in a second step. The active space chosen included the 5*f* and 6*d* shell in a CAS(10,12) calculation. Since the 6*d* shell is more involved in bonding interactions than the 5*f* orbitals, the excitation energies cannot be reproduced properly as larger (oftentimes unaffordable) actives spaces are needed. However, a good molecular orbital analysis can be done in terms of the molecular orbitals involved in vertical electronic transitions.

EXTENDED REFERENCES

1. Izatt, R. M., Haymore, B. L., Bradshaw, J. S. & Christensen, J. J. Facile separation of the cis isomers of dicyclohexyl-18-crown-6. *Inorg. Chem.* **14**, 3132–3133 (2002).
2. Sheldrick, G. M. SHELXT - Integrated space-group and crystal-structure determination. *Acta Crystallogr. Sect. A Found. Crystallogr.* **71**, 3–8 (2015).
3. Dolomanov, O. V., Bourhis, L. J., Gildea, R. J., Howard, J. A. K. & Puschmann, H. OLEX2: A complete structure solution, refinement and analysis program. *J. Appl. Crystallogr.* **42**, 339–341 (2009).
4. te Velde, G. et al. Chemistry with ADF. *J. Comput. Chem.* **22**, 931–967 (2001).
5. Van Lenthe, E., Baerends, E. J. & Snijders, J. G. Relativistic regular two-component Hamiltonians. *J. Chem. Phys.* **99**, 4597–4610 (1993).
6. Greer, R. D. M. et al. Structure and Characterization of an Americium Bis(O,O'-diethyl)dithiophosphate Complex. *Inorg. Chem.* **59**, 16291–16300 (2020).
7. Gaiser, A. N. et al. Creation of an unexpected plane of enhanced covalency in cerium(III) and berkelium(III) terpyridyl complexes. *Nat. Commun.* 2021 121 **12**, 1–9 (2021).

8. Ramanantoanina, H. LFDFT—A Practical Tool for Coordination Chemistry. *Comput.* **10**, 70 (2022).
9. Ramanantoanina, H., Urland, W., Cimpoesu, F. & Daul, C. The angular overlap model extended for two-open-shell *f* and *d* electrons. *Phys. Chem. Chem. Phys*. **16**, 12282–12290 (2014).
10. Judd, B. R. Optical absorption intensities of rare-earth ions. *Phys. Rev.* **127**, 750–761 (1962).
11. Ofelt, G. S. Intensities of crystal spectra of rare-earth ions. *J. Chem. Phys*. **37**, 511–520 (1962).
12. Glendening, E. D., Landis, C. R. & Weinhold, F. NBO 6.0: Natural bond orbital analysis program. *J. Comput. Chem*. **34**, 1429–1437 (2013).
13. Neese, F., Wennmohs, F., Becker, U. & Riplinger, C. The ORCA quantum chemistry program package. *J. Chem. Phys*. **152**, 224108 (2020).

EXTENDED DATA

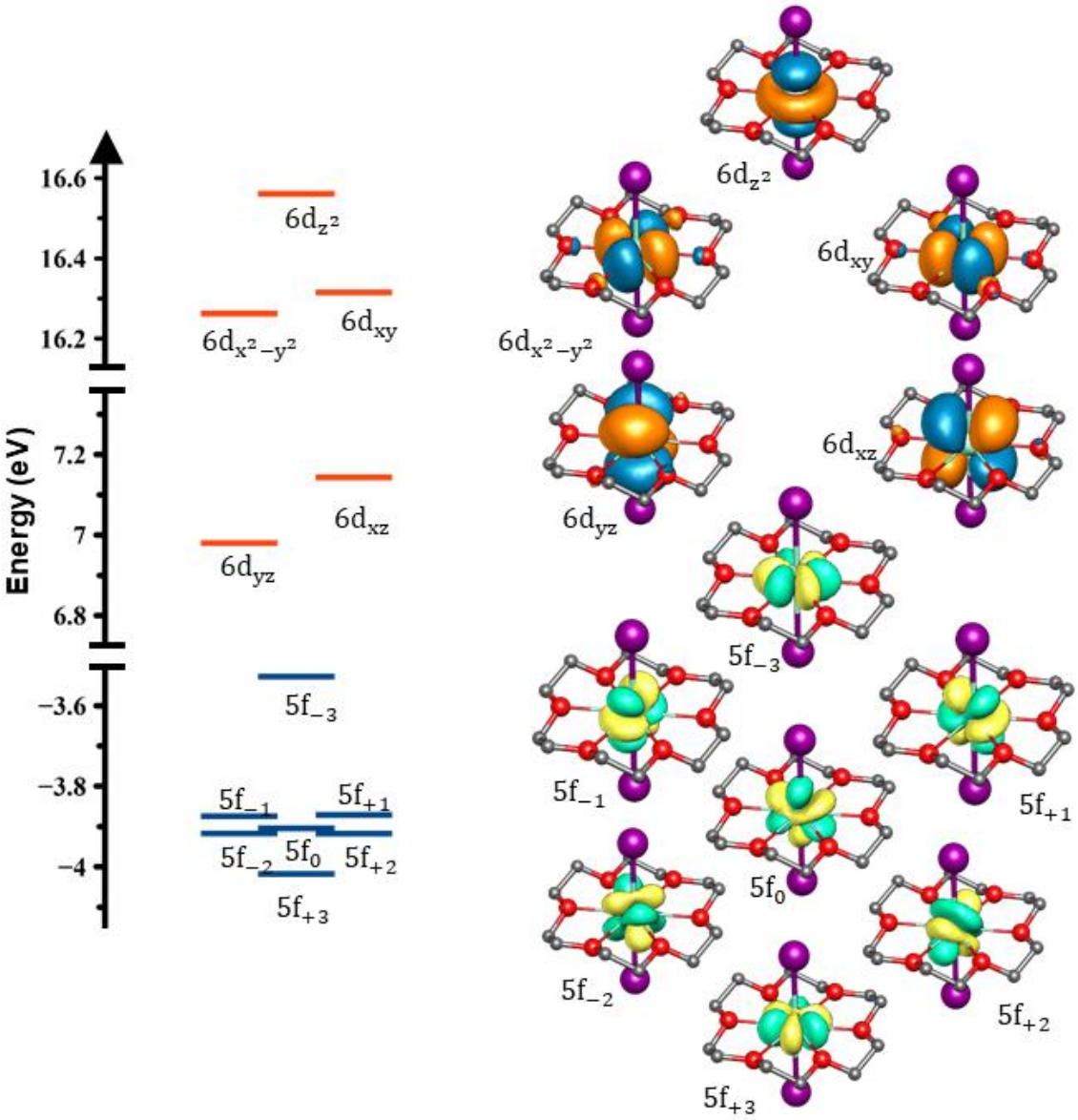

Extended Data Fig. 1: Molecular orbital energy diagram. The orbital splitting obtained from spin-orbit CASSCF calculations, CAS(10,12), is consistent with a pseudo-D_{6h}. Molecular orbitals in the active space are shown.

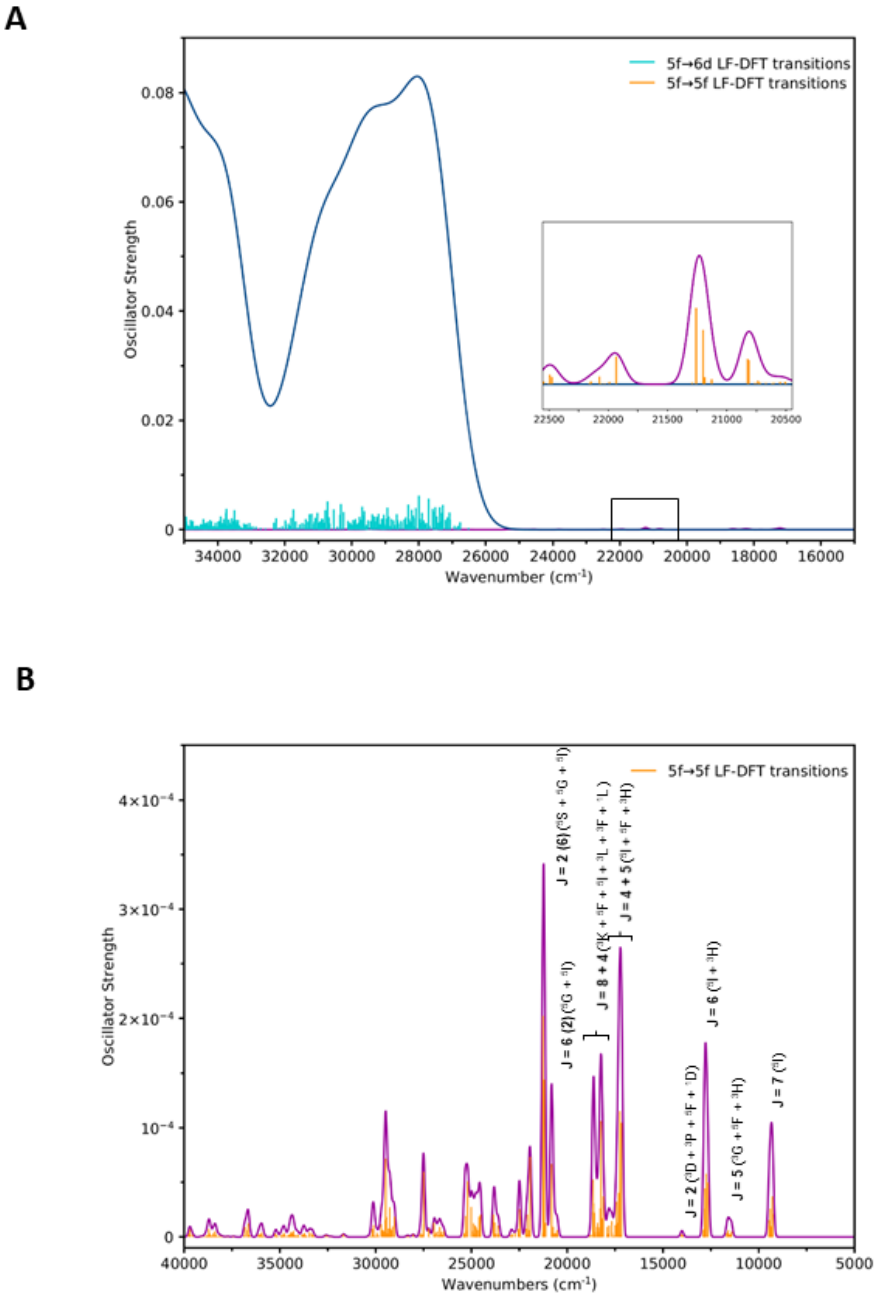

Extended Data Fig. 2: **LFDFT absorption spectroscopy of [Cf^{II}(18-crown-6)(H_2O)$_2$(CH_3CN)]$^{2-}$.** Calculated absorption spectrum using the ligand-field DFT approach, where A) the calculated intensities of the *f-d* transitions obscure most of the *f-f* transitions. The inset corresponds to the most intense *f-f* transition consistent with the experimental spectrum. B) The *f-f* transitions were zoomed in and the lowest lying states assigned. It is clear that the low intensity transitions J = 5 and J = 2 are significantly affected by the ΔS = 0 selection rule, and that there is strong J-mixing (bracketed in bold).

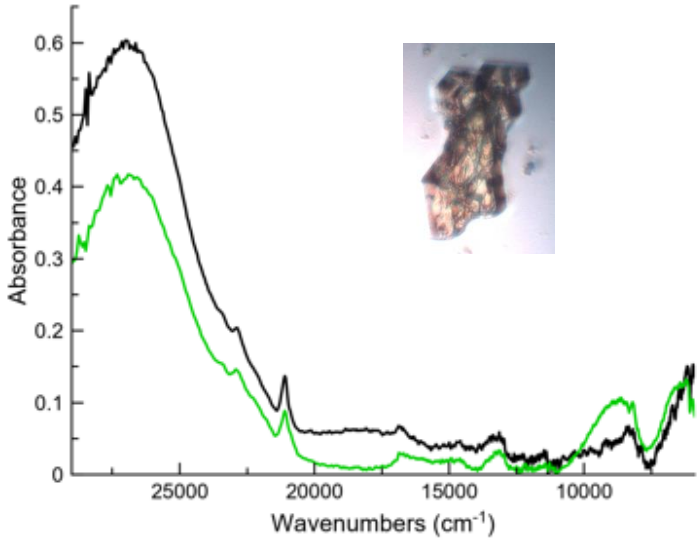

Extended Data Figure 3: Solid-state absorption spectrum of [Cf(18-crown-6)$(H_2O)_{2-x}(CH_3CN)I_x]I_2$. The solid-state absorption spectra for crystals [Cf(18-crown-6)$(H_2O)_{2-x}(CH_3CN)I_x]I_2$ collected at room temperature (green) and 93.15 K (black) possess similar features in the UV region to the broadband features observed in the solution absorption spectrum containing $[Cf(18\text{-crown-6})]^{3+}$ presented in Figure 3.

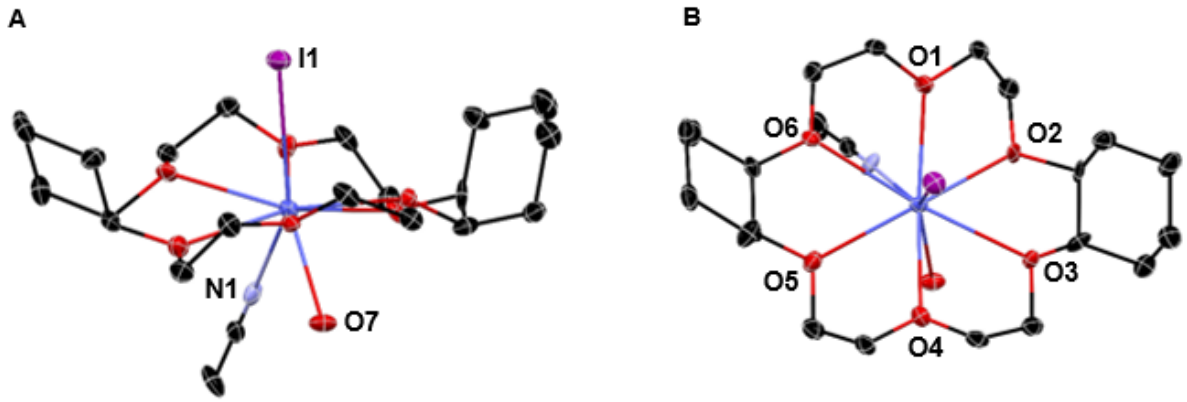

C

M	Am (Å)
Am1-O1	2.543(7)
Am1-O2	2.496(6)
Am1-O3	2.666(6)
Am1-O4	2.527(7)
Am1-O5	2.549(7)
Am1-O6	2.716(7)
Am1-O7	2.427(7)
Am1-I1	3.1107(7)
Am1-N1	2.539(9)

Extended Data Figure 4: Crystal structure of [Am(cis-syn-cis-dicyclohexano-18-crown-6)(H_2O)(CH_3CN)I]I_2 • CH_3CN and associated bond lengths. A) and B) Preparation of AmI_3 • nH_2O (n ≤ 6) can be performed using the same methods reported for CfI_3 • nH_2O (n ≤ 6). Reaction of AmI_3 • nH_2O (n ≤ 6) with dicyclohexano-18-crown-6 and [NBu_4][BPh_4] in acetonitrile yields crystals of [Am(cis-syn-cis-dicyclohexano-18-crown-6)(H_2O)(CH_3CN)I]I_2 • CH_3CN after slow vapor diffusion of diethyl ether. (A) Features a view of the isolated metal complex showing the ligands in apical positions, while (B) shows the coordination of the dicyclohexano-18-crown-6 molecule in the equatorial plane of the molecule. C) A table of bond lengths for the metal complex is provided for comparison with the Cf complexes reported here, as well as similar Am complexes reported in the literature.

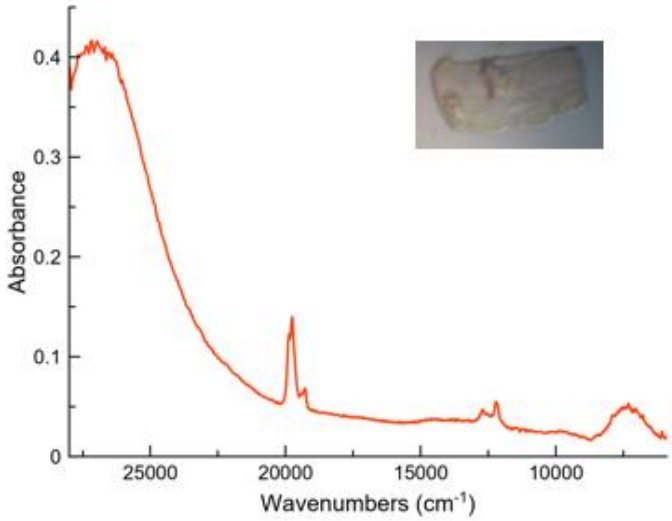

Extended Data Figure 5: Solid-state absorption spectrum of [Am(*cis*-*syn*-*cis*-dicyclohexano-18-crown-6)(H_2O)(CH_3CN)I]I_2 • CH_3CN. Solid-state absorption measurements of [Am(*cis*-*syn*-*cis*-dicyclohexano-18-crown-6)(H_2O)(CH_3CN)I]I_2 • CH_3CN yield characteristic 5*f* → 5*f* transitions exhibited by this compound, namely group E transitions ($^7F_6$) at 19,763 cm^{-1} and hypersensitive group H transitions ($^5L_6$) at 12,207 cm^{-1}.

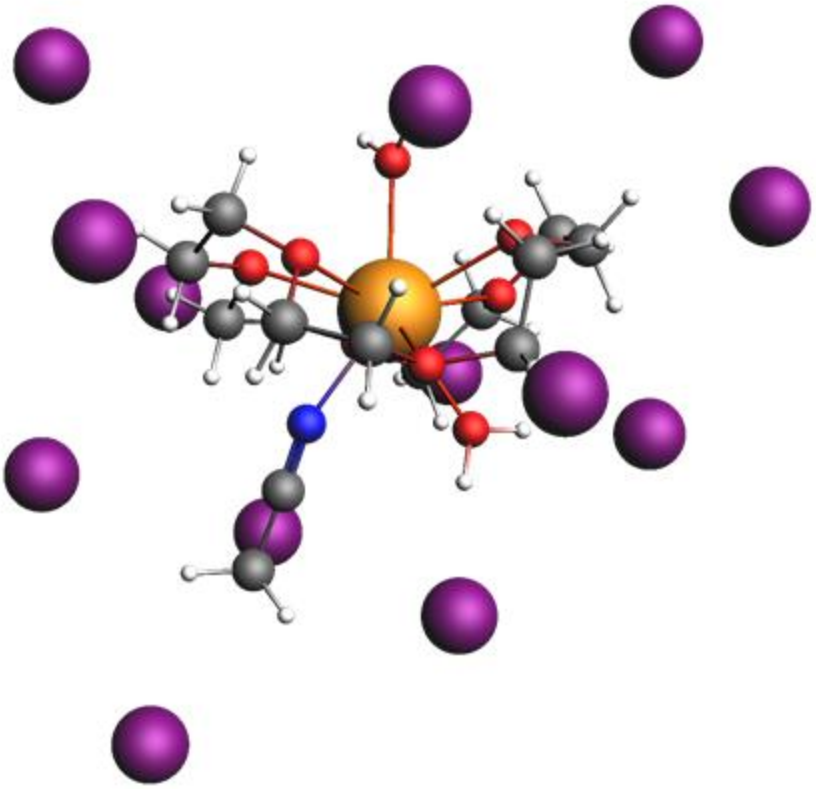

Extended Data Figure 6: Geometry optimization structure. Depiction of the 13 iodide anions considered in the geometry optimization of the **[Cf(18-crown-6)(H_2O)$_{2-x}$(CH_3CN)I_x]** complexes. Their positions were kept fixed in the optimization process.

Extended Data Table 1. Comparison between experimental and optimized Cf – L bond lengths (L = ligand coordinating atom) considering the apical ligand L_{cap} = OH^-, I^-, H_2O. In bold are highlighted the values considered correct for the Cf–L_{cap} bond lengths.

	Experimental	-OH		-I		-OH_2	
Cf – L	OH_2/I^-	No I^-	13 I^-	No I^-	13 I^-	No I^-	13 I^-
O1	2.564(2)	2.653	2.665	2.628	2.573	2.712	2.652
O2	2.514(2)	2.636	2.569	2.609	2.571	2.709	2.588
O3	2.506(2)	2.611	2.546	2.578	2.510	2.706	2.567
O4	2.491(2)	2.598	2.456	2.577	2.464	2.702	2.543
O5	2.489(2)	2.595	2.446	2.573	2.452	2.686	2.508
O6	2.461(2)	2.550	2.444	2.571	2.444	2.641	2.450
O_{avg}	2.504(2)	2.607	2.521	2.589	2.502	2.693	2.551
OH_2	2.413(2)	2.594	2.540	2.524	2.402	2.627	2.413
MeCN	2.535(2)	2.787	2.465	2.616	2.390	2.690	2.387
L_{cap}	2.705(11)/ 2.742(2)	2.098	**2.270**	3.066	**3.164**	2.613	**2.625**